Effect of Dislocations on Performance of LWIR HgCdTe Photodiodes

K. JÓWIKOWSKI and A. ROGALSKI

Institute of Applied Physics, Military University of Technology, 00-908 Warsaw, 2 Kaliskiego Str., Poland

The epitaxial growth of HgCdTe on alternative substrates has emerged as an enabling technology for the fabrication of large-area infrared (IR) focal plane arrays (FPAs). One key technical issue is high dislocation densities in HgCdTe epilayers grown on alternative substrates. This is particularly important with regards to the growth of HgCdTe on heteroepitaxial Si-based substrates, which have a higher dislocation density than the bulk CdZnTe substrates typically used for epitaxial HgCdTe material growth. In the paper a simple model of dislocations as cylindrical regions confined by surfaces with definite surface recombination is proposed. Both radius of dislocations and its surface recombination velocity are determined by comparison of theoretical predictions with carrier lifetime experimental data described by other authors. It is observed that the carrier lifetime depends strongly on recombination velocity; whereas the dependence of the carrier lifetime on dislocation core radius is weaker. The minority carrier lifetime is approximately inversely proportional to the dislocation density for densities higher than 10^5 cm^{-2}. Below this value, the minority carrier lifetime does not change with dislocation density. The influence of dislocation density on the R_oA product of long wavelength infrared (LWIR) HgCdTe photodiodes is also discussed. It is also shown that parameters of dislocations have a strong effect on the R_oA product at temperature around 77 K in the range of dislocation density above 10^6 cm^{-2}. The quantum efficiency is not a strong function of dislocation density.

Key words: Dislocations, HgCdTe, IR detectors

INTRODUCTION

The epitaxial growth of HgCdTe on alternative substrates has emerged as an enabling technology for the fabrication of large-area infrared (IR) focal plane arrays (FPAs). The use of Si substrates is very attractive in IR FPAs technology not only because it is less expensive and available in large area wafers but also because in an FPA structure, the coupling of the Si substrates with Si readout circuitry allows the fabrication of very large arrays exhibiting long-term thermal cycle reliability.

One key technical issue is high dislocation densities in HgCdTe epilayers grown on alternative substrates. This is particularly important with regards to the growth of HgCdTe on heteroepitaxial Si-based substrates, which have a higher dislocation density than the bulk CdZnTe substrates typically used for epitaxial HgCdTe material growth. It is now widely acknowledged that dislocations affect minority carrier lifetime which is directly related to diode performance. The majority of earlier papers were focused on the effect of dislocations and subgrain boundaries on performance of MIS detectors.[1–6] More recently several papers have been published on the effect of dislocation density on the performance of HgCdTe detectors,[7–11] especially photodiodes.[9–11]

In this paper, a numerical model of the influence of dislocations on the minority carrier lifetimes in HgCdTe ternary alloy is presented. In comparison with paper published previously by Johnson et al.[9] where a phenomenological model was developed (based on the conductance of individual and interacting dislocations which shunt the p–n junction), in our paper the dislocations are treated as the regions with magnified carrier recombination. Next, the influence

(Received November 5, 1999; accepted February 5, 2000)

of dislocations on the R_oA product and quantum efficiency, and carrier lifetime of long wavelength infrared (LWIR) HgCdTe photodiodes is analyzed. The predicted theoretical results are compared with available experimental data.

THEORETICAL MODEL

In HgCdTe epitaxial layers there are many dislocations, usually more than about 5×10^4 cm^{-2}. For example, Fig. 1 shows two types of dislocations on (111) and (110) planes. Misfit dislocations caused by lattice mismatch between the substrate and the epilayer are observed on (110) planes perpendicular to the epilayer/substrate interface. The threading dislocations are observed on (111) planes parallel to the interface.

The Coulomb fields associated with the electrically charged dislocation cores act as recombination centers. The presence and amount of charge on a dislocation core depends on the distribution of localized levels in the bandgap in the core and on the Fermi level in the semiconductor. The effective radius of the electrical field is taken to be that distance from the dislocation core within which the field is large enough to move a carrier the distance between dislocations in a minority carrier lifetime as measured in dislocation-free material. In this way, we define a volume within which the lifetime is affected by the presence of a charged dislocation. If the affected volume surrounding all the dislocations is a significant fraction of the total volume, then their presence can affect lifetime and hence R_oA product.

Dislocations are the regions with increasing generation-recombination processes of nonequilibrium carriers. When dislocation density is sufficiently low, the effective minority carrier diffusion length L_D is determined by band-to-band generation-recombination process. It is well known that in the case of LWIR HgCdTe material there are two dominant Auger processes; Auger 1 in the n–type material and Auger 7 in the p–type material. At higher density of dislocations, the effective minority carrier diffusion length L_{eff} is reduced by recombination at dislocations and is described by

$$\frac{1}{L_{eff}^2} = \frac{1}{L_D^2} + \frac{1}{L_{dis}^2} \qquad (1)$$

Hitherto, several simple models have been used to describe influence of dislocations on carrier lifetime. In Landsberg's monograph a barrier model is presented.[12] More recently, Johnson et al.[9] presented very interesting phenomenological model based on the conductance of individual and interacting dislocations which shunt the p–n junction. In our paper the dislocations are treated as the regions with magnified carrier recombination and this type of recombination is included in the generation-recombination terms of transport equations.

We assume that the dislocation pipes with radius of r_o (see Fig. 2) are homogeneously distributed over the entire HgCdTe layer and located parallel to the epilayer/substrate interface. The dislocation cores are surrounded by cylindrical surfaces with radius r_o and r_z. The average interval between dislocation cores is equal $2r_z$. We further assume that some of the charges vanish with recombination velocity, S, at the circumference of the dislocation pipes; at cylindrical surface with radius r_o.

The photoelectrical phenomena in any type of semiconductor device can be analyzed using forward-condition steady-state analysis.[13] Basic equations for d.c. analysis have the well known equations: continuity equations for electrons and holes and Poisson's equation which are collectively referred to as the Van Roosbroeck model:[14]

$$\frac{\partial n}{\partial t} = \frac{1}{q}\mathrm{div}\vec{j}_e + (G - R)_e = 0$$

continuity equation for electrons (2)

$$\frac{\partial p}{\partial t} = \frac{1}{q}\mathrm{div}\vec{j}_h + (G - R)_h = 0$$

continuity equation for holes (3)

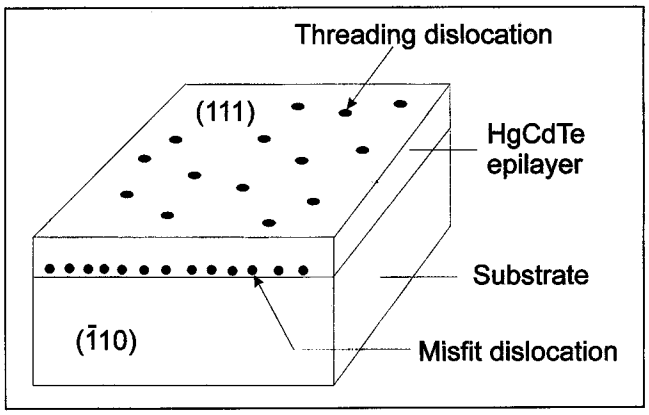

Fig. 1. Schematic picture showing misfit and threading dislocations.

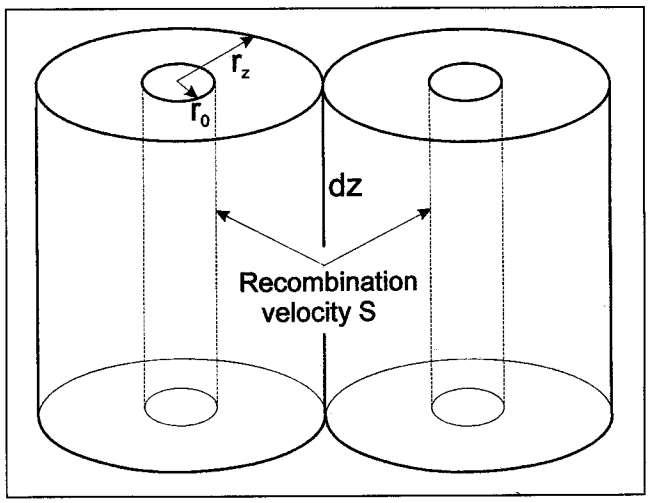

Fig. 2. Model of dislocations as cylindrical regions with the radius r_o confined by surfaces with the definite surface recombination velocity S. The average interval between dislocation cores is equal to $2r_z$.

$$O^{21}1' \_ - \frac{q}{e_n r}(N_d - N. + p - n) - \frac{\Phi}{\text{V POe}_r}$$

Poisson's equation (4)

In the above equations, n and p are the hole and electron concentrations, j_e and $j_{,,}$ are the electron and hole current densities, q is the electron charge, ^{l}P is the electrostatic potential, N_d is the concentration of donors, N_a is the concentration of acceptors, and $e_v e_r$ is the permittivity of the semiconductors. G and R denote the carrier generation and recombination rates, respectively.

The current density can be expressed as a sum of diffusion and drift components

$$j_e = gD_e Vn - g\mu_e nV' \quad (5)$$

$$j_h = gD_{,,}Vp - \%^{l}hPVP \quad (6)$$

where μ_e and μ_h are the electron and hole concentrations, and D_e and D_h are the electron and hole diffusion coefficient.

Equations 5 and 6 can be expressed in a more simple way as a function of the Fermi quasi-level ($D_{,,}$ and 1_h

$$J_e = \text{`1f-`enVTe} \quad (7)$$

$$j_h = qJ_{hP} \quad (8)$$

Many papers devoted to the solution of these equations have been published from papers of Gummel[15] and De Mari[16] down to recently commercially available numerical programs.[17,18] Results from some additional papers[12,19,20] have also been partially regarded in the present paper.

The main problem with Eqs. 2–6 is related to their non-linearity. The carrier concentrations of electrons and holes, the concentrations of ionized impurities, and generation-recombination term (G–R), are rather complicated due to the non-linearity of electrostatic potential Ψ and the Fermi quasi-level Φ. To solve Eqs. 1, 2, and 3 taking into account relations in Eqs. 7 and 8, it is necessary to linearize Eqs. 2–4, 7, 8, and then to calculate Φ_e and Φ_h. The numerical procedure used here is described in Ref. 21. In practice, we start the calculations by solving the Poisson's equation assuming thermodynamic equilibrium. This lead to constant Fermi level across the structure which is then used as the reference energy for further calculations. At the next step, we calculate iteratively the spatial distribution of electrostatic potential, concentrations of electrons, holes, ionized impurities and electron affinity. In the calculation we take into account the non-parabolicity and degeneration. Neumann boundary conditions have been used in calculations of potential at equilibrium conditions. The calculated electrostatic potential at equilibrium is used then to solve Eqs. 2–4 for the non-equilibrium case taking the equilibrium solutions as the initial solutions in the iterative procedure. The electrical bias has been taken into account by the change of the boundary conditions at contact regions. To calculate the influence of illumination we add the optical generation rate to the thermal generation rate. The concentrations and generation-recombination rates in Eqs. 2–4 were expressed as functions of potential and Fermi quasi-levels without any simplified assumptions. The linearization of the iterative equations have been achieved by gradual change of electric bias and optical power density. Apart from dislocation process, band-to-band thermal generation-recombination processes in $Hg_{1-x}Cd_xTe$ (Auger 1 and Auger 7 mechanisms) were taken into account.[22] Modified Anderson[23] expressions have been used to calculate optical absorption as a function of electrostatic potential and Fermi quasi-levels. Remaining material parameters were taken from Ref. 24.

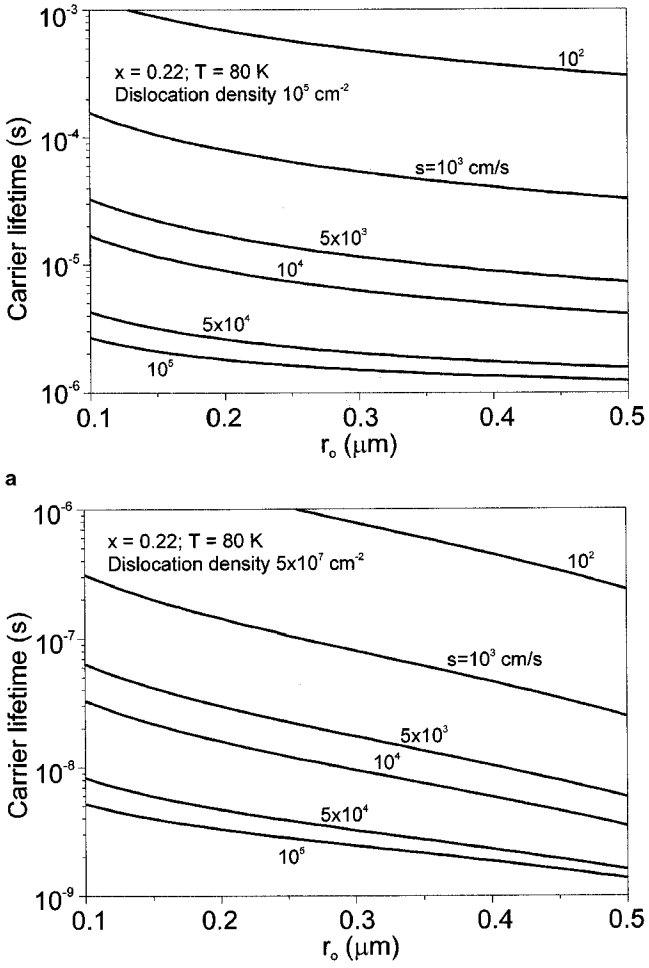

Fig. 3. The dependence of the carrier lifetimes on core radius of dislocations for selected values of recombination velocities at the circumference of the dislocation pipes in $Hg_{0.78}Cd_{0.22}Te$ ternary alloy at 80 K with dislocation density: (a) 10^5 cm^{-2} and (b) 5×10^7 cm^{-2}.

RESULTS OF CALCULATIONS AND DISCUSSION

Figure 3 shows the dependence of the carrier lifetimes on core radius of dislocations for selected values of recombination velocities at the circumference of the dislocation pipes in $Hg_{0.78}Cd_{0.22}Te$ ternary alloy with dislocation density 10^5 cm^{-2} and 5×10^7 cm^{-2} at 80 K.

The same dependence for $Hg_{0.70}Cd_{0.30}Te$ is shown in Fig. 4. For both alloy compositions we observe strong dependence of the carrier lifetime on recombination velocity; whereas the dependence of the carrier lifetime on core radius is weaker.

Using experimental data we can determine two important parameters of dislocations; the radius r_o and the recombination velocity S. Figure 5 shows the dependence of minority carrier lifetime on dislocation density for $Hg_{1-x}Cd_xTe$ ternary alloys with composition x = 0.22 (LWIR MBE grown on GaAs and Si substrates) and x = 0.30 (mid wavelength LPE grown material on CdTe substrates), and carrier concentration of 10^{15} cm^{-3} at temperature 80 K. To achieve good agreement between experimental data and theoretical predictions, the following parameters have been chosen: $r_o = 0.3$ μm and $S = 2 \times 10^4$ cm/s. Clearly the minority carrier lifetime is approximately inversely proportional to the dislocation density for densities higher than 10^5 cm^{-2}. Below this value, the minority carrier lifetime does not change with dislocation density. The experimental dislocation density dependence of the minority carrier lifetime for LPE HgCdTe is descending faster than that of MBE HgCdTe and the dislocation density limit for the constant lifetime is 2×10^5 cm^{-2}, which is lower than that of MBE LWIR HgCdTe. The difference might related to the composition difference rather than the radiative limited recombination mechanism for the carrier concentration of 1×10^{15} cm^{-3} with x = 0.30. In general, however, the values of minority carrier lifetime of LPE HgCdTe deduced from metal-insulator-semiconductor (MIS) devices[3] are in good agreement with the results obtained for MBE LWIR HgCdTe.[25]

Since the minority carrier lifetime influences the R_oA product of photodiode, dislocations should also affect this figure of merit. Two types of HgCdTe photodiode structures are considered: homojunction and double layer heterojunction (DLHJ). In P-on-n (P denotes wider gap) DLHJ photodiode structures, the base n-type layers are sandwiched between substrate (usually CdZnTe) and high-doped, wider-gap regions. Due to backside and internal electric fields (which are "blocking" for minority carriers), influence of surface recombinations on the photodiodes performance is reduced. The influence of surface recombination can be also prevented by the use of suitable passivation. Both optical and thermal generations are suppressed in the P–region due to wide gap. Thus R_oA product of DLHJ structure is higher than homostructure. The thickness of the base region is optimized for near unity quantum efficiency and a low dark current. This is achieved with a base thickness slightly higher than the inverse absorption coefficient for single pass devices: $t = 1/\alpha$ (which is ≈10 μm). Low doping ($n \approx 10^{15}$ cm^{-3}) is beneficial for a low thermal generation and high quantum efficiency. Since the diffusion length in absorbing region is typically longer than its thickness, any carriers generated in the base region can be collected giving rise to the photocurrent.

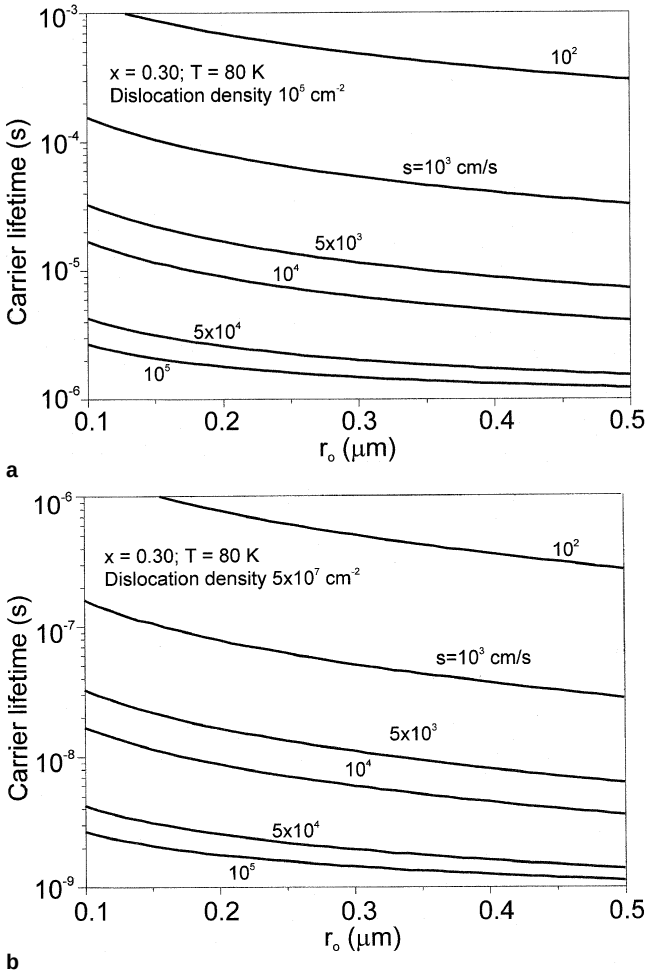

Fig. 4. The dependence of the carrier lifetimes on core radius of dislocations for selected values of recombination velocities at the circumference of the dislocation pipes in $Hg_{0.70}Cd_{0.30}Te$ ternary alloy at 80 K with dislocation density: (a) 10^5 cm^{-2} and (b) 5×10^7 cm^{-2}.

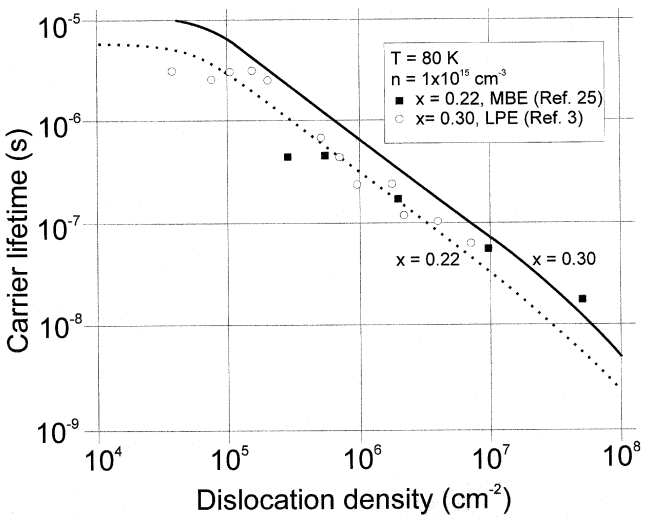

Fig. 5. Dependence of the minority carrier lifetime on dislocation density for LPE (x = 0.30) and MBE (x = 0.22) grown $Hg_{1-x}Cd_xTe$ epilayers at 80 K. Theoretically, calculated curves for alloy composition x = 0.22 (solid line) and x = 0.30 (dashed line) are also shown. In the calculations the following dislocation parameters are assumed: r_o = 0.3 μm and $S = 2 \times 10^4$ cm/s.

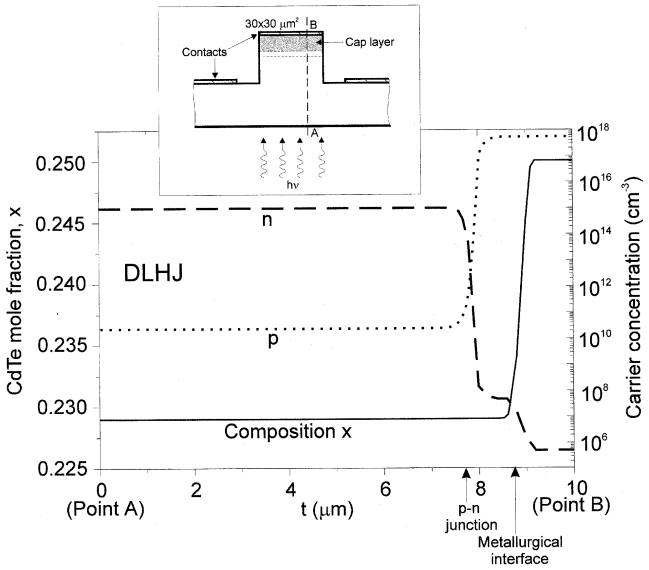

Fig. 6. Geometry, composition profiles, and concentration profiles across the 9.5-μm P-on-n HgCdTe photodiode operated at 77 K. Distribution of particular functions are shown across the line A-B marked in the inside figure.

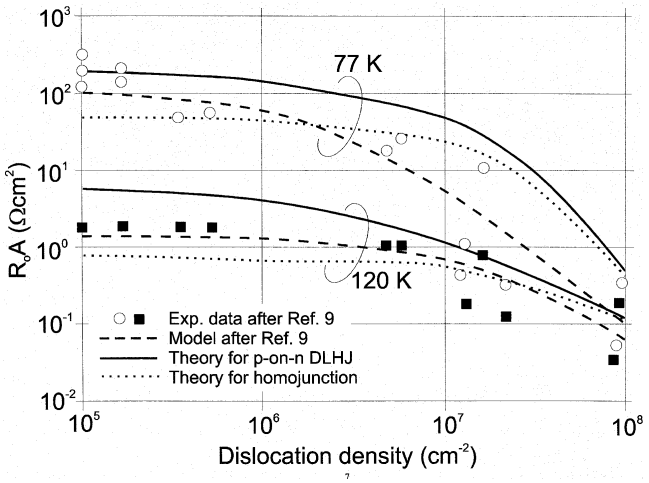

Fig. 7. R_oA product versus dislocation density for 9.5-μm HgCdTe photodiodes at 77 K and 120 K. Experimental data are taken from Ref. 9. The theoretically predicted curves for DLHJ and homojunction HgCdTe photodiodes are also shown.

We also considered the effect of dislocation density on the R_oA product of 9.5-μm P-on-n HgCdTe photodiode operated at 77 K. Figure 6 shows geometry, composition profile, and distribution of carrier concentrations across the line A-B of this photodiode structure. We assume about 1-μm thick P-type cap layer with a carrier concentration 5×10^{17} cm^{-3}. A minimum of the alloy composition step across the heterojunction of about 0.2 is needed to suppress diffusion current from the P-type cap layer. The electrical junction is positioned near the metallurgical interface and it is wise to place the junction in the small band gap layer to avoid deleterious effects on the quantum efficiency and dark currents.

Figure 7 shows a plot of R_oA of 9.5-μm DLHJ photodiodes versus dislocation density measured at 120 K and 77 K at zero field of view. It was assumed

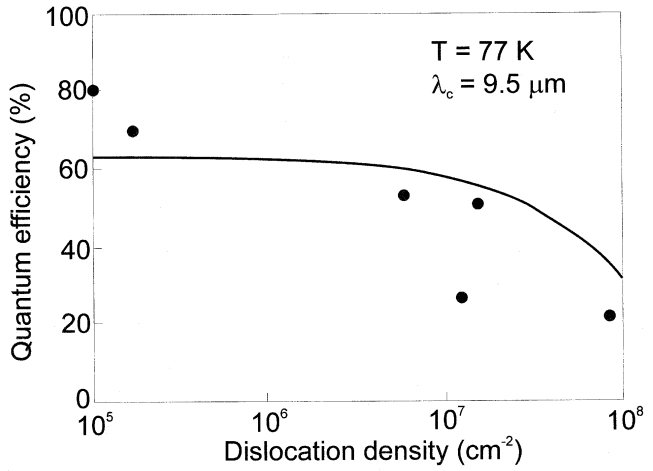

Fig. 8. Quantum efficiency versus dislocation density measured at 78 K for 9.5-μm DLHJ HgCdTe photodiodes at 78 K. Experimental results are taken from Ref. 9.

in calculations that $r_o = 0.3$ μm and $S = 2 \times 10^4$ cm/s. At 77 K, R_oA begins to decrease at dislocation density of approximately 10^6 cm^{-2}, while at 120 K this dependence is weaker. In general, good agreement has been obtained between theoretically predicted R_oA product and experimental data. The scatter in the R_oA data at large dislocation density may be associated with the presence of an increased number of pairs of interacting dislocations. It is expected that these pairs are more effective in reducing R_oA than individual dislocations.[9] The scatter in the R_oA data at a given dislocation density also decreases substantially as the measurement temperature increases and the diodes go from being limited by tunneling and g-r currents at lower temperature to being dominated by diffusion currents at 120 K. In addition, Fig. 7 compares the theoretical curves obtained by Johnson et al.[9] with our results calculated for DLHJ photodiodes and homojunction photodiodes. We can notice that the first two kinds of calculations ensure better agreement with experimental results. It is also confirmed that theoretically predicted values of R_oA product for DLHJ structures are higher than for homostructures.

The last figure (Fig. 8) shows the dependence of quantum efficiency on dislocation density for 9.5-μm DLHJ HgCdTe photodiodes at 77 K. The quantum efficiency is a weak function of dislocation density up to approximately 10^7 cm^{-2}. This conclusion has been previously experimentally confirmed by Johnson et al.[9] Thus, unlike the electrical properties of the photodiodes (R_oA product), the quantum efficiency is not strongly affected by dislocations.

CONCLUSIONS

It is well established that dislocations originating from material growth affect the performance of HgCdTe photodiodes. A quantitative understanding of the effect of dislocations on the electrical and optical properties of photodiodes is needed to establish their role in determining detector performance. In the paper a simple model of dislocations as cylindrical regions confined by surfaces with definite surface

recombination is proposed. Both radius of dislocations and its surface recombination velocity are determined by comparison of theoretical predictions with carrier lifetime experimental data described by other authors.

There exists a strong dependence of the carrier lifetime on recombination velocity. The dependence of the carrier lifetime on dislocation core radius is much weaker. The minority carrier lifetime is approximately inversely proportional to the dislocation density for densities higher than 10^5 cm^{-2}. Below this value, the minority carrier lifetime does not change with dislocation density. Finally, it is also shown that parameters of dislocations can have a strong effect on R_oA product of LWIR HgCdTe photodiodes at temperature around 77 K. The dependence of quantum efficiency on dislocation density is weaker.

ACKNOWLEDGEMENT

This paper was partially supported by the KBN (Poland) under grant numbers PBZ 28.11/P6 and 8T11B054-15.

REFERENCES

1. A.J. Syllaios and L. Colombo, *Proc. IEDM 1982* (New York: IEDM, 1982), p. 137.
2. H.F. Schaake, J.H. Tregilgas, A.J. Lewis, and P.M. Everett, *J. Vac. Sci. Technol. A* 1, 1625 (1983).
3. T. Yamamoto, H. Sakai, and K. Tanikawa, *J. Cryst. Growth* 72, 270 (1985).
4. Y. Miyamoto, H. Sakai, and K. Tanikawa, *Proc. SPIE* 572, 115 (1985).
5. D. Chandra, J.H. Tregilgas, and M.W. Goodwin, *J. Vac. Sci. Technol. B* 9, 1852 (1991).
6. R.S. List, *J. Vac. Sci. Technol. B* 10, 1651 (1992).
7. M.J. Maachowski, J. Piotrowski, and A. Rogalski, *Infrared Physics* 28, 279 (1988).
8. M.J. Maachowski, J. Piotrowski, and A. Rogalski, *Phys. Stat. Sol. (a)* 113, 467 (1989).
9. S.M. Johnson, D.R. Rhiger, J.P. Rosbeck, J.M. Peterson, S.M. Taylor, and M.E. Boyd, *J. Vac. Sci. Technol. B* 10, 1499 (1992).
10. A.T. Paxton, A. Sher, M. Berding. M. Van Schilfgaard, and M.W. Muller, *J. Electron. Mater.* 24, 525 (1995).
11. M.C. Chen, R.S. List, D. Chandra, M.J. Bevan, I. Colombo, and H.F. Schaake, *J. Electron. Mater.* 25, 1375 (1996).
12. P.T. Landsbert, *Recombination in Semiconductors* (Cambridge, U.K.: Cambridge University Press, 1991).
13. M. Kurata, *Numerical Analysis of Semiconductor Devices* (Toronto, Canada: Lexington Books, 1982).
14. W. Van Roosbroeck, *Bell. Syst. Technol. J.* 29, 560 (1950).
15. H.K. Gummel, *IEEE Trans. Electron Devices* ED11, 455 (1964).
16. A. de Mari, *Solid State Electron.* 11, 1021 (1968).
17. *Semicond. Devices* (software) (CA: Dawn Technologies, Inc.).
18. *Apsys* (software) (Ontario, Canada: Crosslight Software, Inc.).
19. D.L. Scharfetter and H.K. Gummel, *IEEE Trans. Electron Devices* ED16, 64 (1969).
20. W.L. Engl, H.K. Dirks, and B. Meinerzhagen, *Proc. IEEE* 71, (1983).
21. K. Jówikowski, *Biul. WAT* 7/8, 161 (1998) (in Polish).
22. V.C. Lopes, A.J. Syllaios, and M.C. Chen, *Semicond. Sci. Technol.* 8, 824 (1993).
23. W.W. Anderson, *Infrared Phys.* 20, 363 (1980).
24. A. Rogalski, *Infrared Photon Detectors* (Bellingham, WA: SPIE Optical Engineering Press, 1995).
25. S.H. Shin, J.M. Arias, D.D. Edwall, M. Zandian, J.G. Pasko, and R.E. DeWames, *J. Vac. Sci. Technol. B* 10, 1499 (1992).